Shell structure and phase relations in electronic properties of metal nanowires from an electron-gas model

Yong Han[1,*] and Da-Jiang Liu[2]
[1]*Institute of Physical Research and Technology, Iowa State University, Ames, Iowa 50011, USA*
[2]*Ames Laboratory-U.S. DOE, Iowa State University, Ames, Iowa 50011, USA*
(Received 9 August 2009; revised manuscript received 18 August 2010; published 10 September 2010)

The electronic and dynamic properties of metal nanowires are analyzed by using a minimal electron-gas model (EGM), in which the nanowire is treated as a close system with variable Fermi energy as a function of nanowire radius. We show that the planar surface energy and the curvature energy from the EGM are reasonably consistent with those from previous stabilized-jellium-model calculations, especially for metals with low electron densities. The EGM shell structure due to the fillings of quantum-well subbands is similar to that from the stabilized jellium model. The crossings between subbands and Fermi energy level for the metal nanowire correspond to cusps on the chemical-potential curve versus nanowire radius, but inflection points on the surface-free-energy curve versus the radius, as in the case of metal nanofilms. We also find an oscillatory variation in electron density versus radius at the nanowire center with a global oscillation period which approximately equals half Fermi wavelength. Wire string tension, average binding energy, and thermodynamic stability from the EGM are in good agreement with the data from previous first-principles density-functional theory calculations. We also compare our model with those from previous reported free-electron models, in which the nanowire is treated as an open system with a constant Fermi energy. We demonstrate that the fundamental thermodynamic properties depend sensitively on the way that the potential wall is constructed in the models.

DOI: 10.1103/PhysRevB.82.125420 PACS number(s): 73.21.Hb, 61.46.Km, 62.23.Hj, 73.63.Nm

I. INTRODUCTION

Metal nanoclusters can be modeled by the electron confinement in a geometrically symmetric potential well, exhibiting the shell structures in physical properties.[1–7] For metal nanofilms, the confinement of electrons along the direction perpendicular to film surface leads to the periodic oscillations of electronic properties as function of film thickness.[8–10] Similarly, for a metal nanowire, the radial [spatially two-dimensional (2D)] quantum confinement of electrons leads to the oscillations of electronic properties as a function of wire radius, and correspondingly, this oscillation spectrum can be referred to as the 2D shell structure. The size dependency of physical properties of nanostructures has been known as the quantum size effect (QSE). Various experiments[11,12] and theoretical modelings[13–15] show that some radii of nanowires with certain microscopic configurations can be particularly thermodynamically stable, and in contrast, there are no stable nanowires observed in some specific regions of radii, which are therefore called the "stability gaps."[16] Experimental measurements also reveal quantization of electrical conductance in nanowires.[17–19]

Jellium-based models[20,21] can effectively describe the energetics, dynamic properties, and electric transport properties of metal nanowires. For example, the total energy per unit length oscillates as a function of the wire radius, reflecting the electronic shell structure of the system.[22,23] In all these studies, the nanowire is treated as a closed system. On the other hand, the metal nanowire is also treated as an open system in the free-electron model.[24–29] In calculations of thermodynamic properties, various assumptions about the compressibility of the electron gas during its deformation can lead to significant difference in macroscopic properties. Urban *et al.*[30,31] proposed to exploit this sensitivity by fitting the free-electron model to specific materials. However, as a comparison with the open system, an extensive study of the free-electron model, in which the metal nanowire is treated as a closed system, is still lacking.

In this paper, we present a detailed study of electronic and dynamic properties of metal nanowires using the electron-gas model (EGM) with an infinitely long cylindrical hard-wall potential well. For a closed system, the number of electrons is fixed while the radius of potential well is appropriately chosen and the chemical potential (i.e., Fermi energy level) will be determined as a function of the radius. For an open system, the Fermi energy level is fixed while the number of the electrons will be determined and it is radius dependent. In Sec. II, we describe the details of our model. In Sec. III, we first make an analysis for the asymptotic behavior toward large radii of the metal nanowire based on the Weyl expansion. We will show the difference in planar surface energy and curvature energy for both the closed and open systems with different potential-well-boundary choices. Then, we discuss the oscillation behavior (shell structure) of various physical properties, mainly focusing on the closed system. The analysis for the shell structure reveals that there is a certain phase relation between the surface free energy and the subband crossings, generalizing the results for metal nanofilms.[9,10] We show that for incompressible electron gas, the subband crossings correspond to the inflection points on the surface free energy curve versus radius. However, for completely compressible electron gas in an open system, the subband crossings correspond to the cusp positions on the surface-free-energy curve versus radius. Finally we compare the results from our model with the existing data from first-principles density-functional theory (DFT) calculations. Section IV gives the conclusion.

FIG. 1. (Color online) Schematic illustration of a metal electron-gas nanowire in a square-well potential with the surface-charge neutrality requirement. The dashed cylinder represents the geometrical surface of the metal wire while the thick solid cylinder represents the potential boundary.

II. MODEL

As in a jellium model, we assume that the positive charge is uniformly distributed within a cylindrical nanowire with infinite length. The boundary of potential well is at a distance b from the jellium edge, as shown in Fig. 1. The effective potential is simplified by an infinite barrier, i.e., the hard-wall potential, and has the form

$$U_{\text{eff}} = \begin{cases} 0, & \text{for } \rho < r, \\ \infty, & \text{for } \rho > r, \end{cases} \tag{1}$$

where $r \equiv R+b$ is the radius of potential well and R is the geometric radius of the wire. The physical motivation of b is that in the jellium model for metal surface, electrons spill over the boundary of the positive-charge distribution. Another perspective is that for electrons in a hard-wall potential, there is depletion region near the hard-wall boundary. For a half-infinite surface, Bardeen[32] shows that by imposing a zero surface-charge condition, the value of b is uniquely determined by the potential-well height U_0. Specifically $b=0$ for $U_0=E_F$ (the bulk Fermi energy) and $b=3\lambda_F/16$ for $U_0=\infty$. We note that the result of $b=3\lambda_F/16$ can be also derived from the Weyl expansion for the density of eigenmodes in a cavity with Dirichlet boundary conditions.[33] More on this important parameter will be discussed later.

Solving the Schrödinger equation for a cylinder (supercell) with length L, which is periodic along the central axis (as the z direction in cylindrical coordinates ρ, φ, z) of the nanowire, one can obtain the single-electron wave functions as[16]

$$\psi_{n,l,k_z}(\rho,\varphi,z) = \frac{1}{r\sqrt{\pi L} J_{l+1}(\zeta_{n,l})} J_l\left(\frac{\rho\zeta_{n,l}}{r}\right) e^{i(l\varphi+k_z z)}, \tag{2}$$

where $\zeta_{n,l}$ is the nth zero of the Bessel function $J_l(x)$ with order $l=0, \pm 1, \pm 2, \ldots$, and $n=1,2,3,\ldots$; $k_z=2\pi l_z/L$ with $l_z=0, \pm 1, \pm 2, \ldots$. The eigenenergies are

$$\varepsilon_{n,l} = \frac{\hbar^2}{2m_e}\frac{\zeta_{n,l}^2}{r^2} \equiv \frac{\hbar^2}{2m_e}k_{n,l}^2, \tag{3}$$

where m_e is the mass of an electron.

In **k** space, the states (i.e., the quantum-well subbands) occupied by electrons compose a series of Fermi "rungs," as shown in Fig. 2, defined by

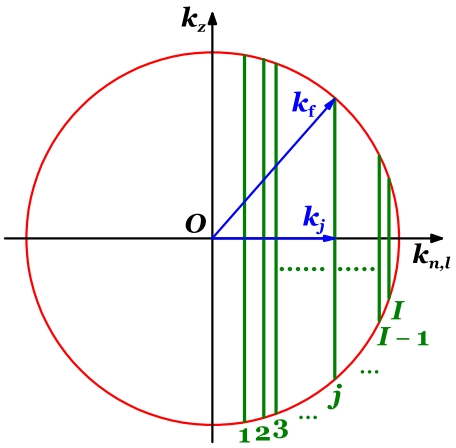

FIG. 2. (Color online) The states occupied by electrons, illustrating as a series of Fermi rungs (green) within the Fermi circle (red).

$$k_z^2 \le k_f^2 - k_j^2, \quad j_{n,|l|} = 1,2,\ldots,I, \tag{4}$$

where $j_{n,|l|}$ (hereafter referred to as j) denotes the quantum numbers $(n,|l|)$ with a rearrangement in an order from small to big values of $\zeta_{n,|l|}$, and the Fermi energy $\varepsilon_f=\hbar^2k_f^2/(2m_e)$ is defined as the highest occupied energy level, which corresponds to the radius of the Fermi circle. It follows that the maximum number I of Fermi rungs can be determined by $\varepsilon_I \le \varepsilon_f < \varepsilon_{I+1}$. Taking advantage of these Fermi rungs, the total number of electrons can be obtained as

$$N = \sum_{j=1}^{I} 2\delta_l \sqrt{k_f^2 - k_j^2}\frac{L}{\pi}, \tag{5}$$

where $\delta_l=1$ for $l=0$ (twofold degeneracy) and $\delta_l=2$ for other $|l|$ (fourfold degeneracy).

For a metal nanowire with zero electric charge, the number of electrons is valency times the number of positive ions, and therefore determined by the geometric radius R of the nanowire. In free-electron models, the positive ions is not explicitly referenced, instead one can define the geometric radius to satisfy the relation

$$N \equiv \pi R^2 L w_{\text{bulk}}, \tag{6}$$

where $w_{\text{bulk}} \equiv k_F^3/(3\pi^2) \equiv 8\pi/(3\lambda_F^3)$ is the average electron density for bulk metal.[10] Then, from Eqs. (5) and (6), one can obtain a relation for ε_f of the form

$$\frac{2\pi^2}{3}\Xi^2 = \sum_{j=1}^{I} \delta_l \sqrt{\frac{\varepsilon_f}{E_F} - \frac{\zeta_j^2}{4\pi^2\xi^2}}, \tag{7}$$

where $\Xi \equiv R/\lambda_F$, $\xi \equiv r/\lambda_F$, and the bulk-metal Fermi energy $E_F \equiv \hbar^2k_F^2/(2m_e)$.

By means of Fig. 2, the total energy E of supercell can be calculated as

$$E = 2\sum_{j=1}^{I} \delta_l \int_0^{k_m} \frac{\hbar^2}{2m_e}(k_z^2 + k_j^2)\frac{L}{\pi}dk_z, \tag{8}$$

where $k_m \equiv \sqrt{k_f^2 - k_j^2}$. Completing the integration of Eq. (8) and performing necessary algebraic operation yields

$$\frac{E}{E_F} = \frac{4L}{3\lambda_F}\sum_{j=1}^{I} \delta_l \left(\frac{\varepsilon_f}{E_F} + \frac{\zeta_j^2}{2\pi^2\xi^2}\right)\sqrt{\frac{\varepsilon_f}{E_F} - \frac{\zeta_j^2}{4\pi^2\xi^2}}. \tag{9}$$

From the wave functions of Eq. (2) and by means of Fig. 2, the electron-density distribution $w(\rho,\varphi,z)=w(\rho)$ can be obtained as

$$\frac{w}{w_{\text{bulk}}} = \frac{3}{2\pi^2\xi^2}\sum_{j=1}^{I} \frac{\delta_l}{J_{l+1}^2(\zeta_j)}\sqrt{\frac{\varepsilon_f}{E_F} - \frac{\zeta_j^2}{4\pi^2\xi^2}} J_l^2\left(\frac{\rho\zeta_j}{r}\right). \tag{10}$$

Equations (5) and (7) can be applied to both a closed and an open system. For a closed system, i.e., the metal nanowire is considered as a canonical ensemble, N or R is a known variable, and one needs to solve for ε_f by using Eq. (7). Here, we also need to know the value of $r=R+b$. As mentioned above, for $R\to\infty$, b should be equal to $3\lambda_F/16$ to avoid net surface charge. However, for finite R, b cannot be uniquely determined from the charge-neutrality requirement, as one can freely choose ε_f. Here, as a minimal model, we assume b to be a certain constant $\bar{b}$ and $\bar{b}$ is set to be $3\lambda_F/16$, i.e., the value for a planar semi-infinite plane.[10] Such model is referred as to the "constant-b model" hereinafter.

The excess energy due to the formation of surface is given by

$$E_s \equiv 2\pi RL\gamma = E - N\sigma_{\text{bulk}}, \tag{11}$$

where γ is defined as the surface free energy per unit area and $\sigma_{\text{bulk}} \equiv 3E_F/5$ is the per electron energy for bulk-metal electron gas. The per electron energy for the metal nanowire can be calculated as $\sigma=E/N$ with N and E expressed in Eqs. (6) and (9), respectively. The string tension (i.e., excess energy per unit length)[14] is calculated as $f=E_s/L=2\pi R\gamma$. In the following sections, we will discuss these quantities.

In a grand-canonical ensemble (open system), the number of electrons are variable while the Fermi energy ε_f is fixed. N and E can be directly obtained from Eqs. (5) and (9) by setting $k_f=k_F$ and $\varepsilon_f=E_F$. The grand-canonical potential can be defined as

$$\Omega = E - NE_F \tag{12}$$

and the excess grand potential due to the formation of surface is given by

$$\Omega_s = \Omega - \bar{V}w_{\text{bulk}}\omega_{\text{bulk}}, \tag{13}$$

where $\omega_{\text{bulk}}=\sigma_{\text{bulk}}-E_F=-2E_F/5$ and $\bar{V}$ is the volume of the nanowire within a properly chosen dividing surface. The surface can only be unambiguously defined for a planar semi-infinite surface. In previous studies,[27] a macroscopic number of electrons, $\bar{N}$, is also defined and could be understood through the relation $\bar{N}=w_{\text{bulk}}\bar{V}$.

III. RESULTS AND DISCUSSION

A. Asymptotic behavior

Before we discuss the shell structure of the metal nanowire, it is instructive to look at the asymptotic behavior for large radii. The Weyl expansion is invaluable for this purpose. For a smooth cavity, the wave-number density of eigenmodes with the Dirichlet boundary condition is given by[33]

$$g(k) = \frac{k^2}{2\pi^2}\mathcal{V} - \frac{k}{8\pi}\mathcal{S} + \frac{1}{6\pi^2}\mathcal{C}, \tag{14}$$

where $\mathcal{V}$ and $\mathcal{S}$ are the volume and the surface area of the cavity, respectively; $\mathcal{C}$ is the surface mean curvature, which is defined as the surface integral over the arithmetic mean of two-principle curvatures, K_1 and K_2, i.e., $\int dA\frac{1}{2}(K_1+K_2)$. For a cylindrical nanowire, one has $\mathcal{V}=\pi r^2L$, $\mathcal{S}=2\pi rL$, and $\mathcal{C}=\pi L$. The number of electron is then given as

$$N \approx \int_0^{k_f} 2g(k)dk, \tag{15}$$

where the factor of 2 is due to spin degeneracy of electrons.

Considering the constant-b model with $r=R+\bar{b}$, from Eq. (15), we obtain

$$\frac{\varepsilon_f}{E_F} = 1 + \left(\frac{1}{4} - \frac{4}{3}\bar{\beta}\right)\Xi^{-1} + \left(\frac{3}{64} - \frac{5\bar{\beta}}{12} + \frac{14\bar{\beta}^2}{9} - \frac{1}{6\pi^2}\right)\Xi^{-2} + O(\Xi^{-3}), \tag{16}$$

where $\bar{\beta} \equiv \bar{b}/\lambda_F$. By letting $\bar{\beta}=3/16$ and neglecting the high-order terms $O(\Xi^{-3})$ for large radii, Eq. (16) becomes

$$\frac{\varepsilon_f}{E_F} \approx 1 + \frac{0.00655}{\Xi^2}. \tag{17}$$

Note that there is no Ξ^{-1} correction in Eq. (17). The asymptotic behavior of ε_f versus Ξ from Eq. (17) is plotted in Fig. 3 [the black curve in the inset of Fig. 3(a)].

For the excess energy, it is useful to separate it into a planar surface-energy term and curvature energy term when the liquid-drop model[34] is used. Then, in the case of a nanowire, one has

$$E_s = \gamma_p S + \frac{1}{2}\gamma_c C, \tag{18}$$

where S is the surface area and C the mean surface curvature with a suitably chosen boundary. Here we use the *geometric* boundary of the nanowire as the dividing surface, and then $S=2\pi RL$ and $C=\pi L$. Using Eq. (11) with the total energy

$$E = \int_0^{k_f} 2g(k)\frac{\hbar^2}{2m_e}k^2dk, \tag{19}$$

one can obtain the excess energy E_s. Neglecting the high-order terms $O(\Xi^{-1})$ of E_s for large radii and comparing with Eq. (18) yields

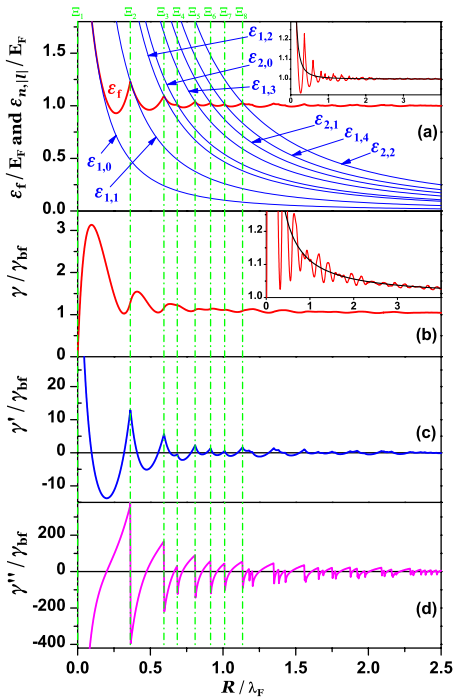

FIG. 3. (Color online) (a) Fermi energy level ε_f and eigenenergies $\varepsilon_{n,|l|}$, (b) surface free energy γ, (c) first derivative of γ, and (d) second derivative of γ versus nanowire radius R. Subband crossings are marked by green vertical dashed-dotted lines. The insets in (a) and (b) are the rescalings of (a) and (b) with the black solid curves from the asymptotic formulas of Eqs. (17) and (22), respectively.

$$\gamma_p = \frac{\pi E_F}{\lambda_F^2}\left(\frac{1}{4} - \frac{32}{30}\bar{\beta}\right) \tag{20}$$

and

$$\gamma_c = \frac{E_F}{\lambda_F}\left(\frac{\pi}{4} - \frac{8}{9\pi} - \frac{5}{3}\pi\bar{\beta} + \frac{224}{45}\pi\bar{\beta}^2\right). \tag{21}$$

Note that γ_c is always positive for any $\bar{\beta} \geq 0$. For $\bar{\beta}=3/16$, one has $\gamma_p = \pi E_F/(20\lambda_F^2) \equiv \gamma_{bf}$ (i.e., the surface free energy corresponding to the bulk film[10]), and $\gamma_c = 0.0705 E_F/\lambda_F$. Thus, considering Eqs. (11) and (18), one can obtain

$$\gamma = \gamma_p + \frac{\gamma_c}{4R} \approx \gamma_{bf}\left(1 + \frac{0.1122}{\Xi}\right). \tag{22}$$

The asymptotic behavior of γ versus Ξ from Eq. (22) is plotted in Fig. 3 [the black curve in the inset of Fig. 3(b)]. To compare the results from the above analysis with previous stabilized jellium model (SJM), in Table I we list γ_p and γ_c from Perdew *et al.*,[35] Ziesche *et al.*,[36] and in Eq. (22). The agreement is satisfactory, and particularly, the agreement for Na and Cs is better than Al, indicating that the noninteracting electron-gas model is a good approximation to the interacting jellium model for the low-electron-density metals, see Table I for the bulk-metal average electron-density w_{bulk} values of Al, Na, and Cs.

For the grand-canonical ensemble with constants $\varepsilon_f = E_F$ and $k_f = k_F$ in Eqs. (15) and (19), the result for N and Ω are already obtained by Stafford *et al.*[27] For the surface excess grand potential, one needs to determine the dividing surface satisfying $\bar{N} = \bar{V}/w_{bulk}$. A natural choice for $\bar{N}$ is the expression of N derived from the Weyl expansion.[27] Using this choice, one can easily show that

$$\frac{\Omega_s}{E_F L/\lambda_F} \approx \frac{\pi^2 \xi}{10} - \frac{8}{45}, \tag{23}$$

where $\xi \equiv r/\lambda_F$. This particular result for the EGM in a grand ensemble was derived previously in Ref. 29. Note that the linear term of r in Eq. (23) is the same as that of the constant-b model with $b = 3\lambda_F/16$, but the constant term (which is related to the curvature energy) is now negative. More results with a parametrized constraint (the generalization of the Weyl-expansion expression) are also obtained in Ref. 31.

It should be also noted that the planar surface energy γ_p is rather sensitive to the choice of $\bar{\beta}$ as indicated in Eq. (20), e.g., when $\bar{\beta}=0$ is chosen, i.e., the potential wall coincides with the geometric wall (no electronic charge spilling), the γ_p value becomes five times as big as that of $\bar{\beta}=3/16$. In contrast to the results of taking $\bar{\beta}=0$ in the EGM, taking $\bar{\beta}=3/16$ as a benchmark value seems to be rather reasonable when we compare the result from the EGM with those from the SJM and first-principles DFT calculations, as will be shown in the following sections.

On the other hand, the curvature energy in the EGM depends on the details of the model, which can be ambiguous for a metal nanowire. For example, for the canonical-ensemble model, while it is certain that b should approach $3\lambda_F/16$ as $R \to \infty$ to avoid the surface charge, the assumption of $b=\bar{b}$ is less well justified. Similarly, in the grand-canonical-ensemble model, there can be other reasonable choices for the Gibbs surface that can give different curva-

TABLE I. Planar surface energy γ_p and curvature energy γ_c from the SJM (Refs. 35 and 36) and our asymptotic analysis [Eq. (22)]. Wigner-Seitz radius r_s is in unit of Bohr radius a_B; bulk-metal average electron density w_{bulk} is in unit of $a_B^{-3} \times 10^{-3}$; γ_p and γ_c are in units of meV/a_B^2 and meV/a_B, respectively.

Metal	r_s	w_{bulk}	γ_p in Ref. 35	γ_p in Ref. 36	γ_p in Eq. (22)	γ_c in Ref. 35	γ_c in Ref. 36	γ_c in Eq. (22)
Al	2.07	26.92	16.19	16.15	40.00	49.8	44.5	121.64
Na	3.93	3.933	3.13	3.14	3.78	9.84	9.54	17.77
Cs	5.62	1.345	1.03	1.06	0.74	3.67	3.84	6.08

ture energies. At this stage, it is unclear to us whether an unambiguous curvature energy can be derived in the EGM.

Finally, we note that the choice of different constraints during metal deformation has been proposed to adapt the EGM to specific materials in Ref. 31. It will be interesting to explore this concept and apply it to the canonical-ensemble model also. The planar surface energy and curvature energy for the metals with high electron density cannot be well described by the constant-b model, as discussed above, even though the value of $\bar{b}$ is, in principle, adjustable. For example, considering the slightly larger charge spilling for the high-electron-density metals,[37] we can choose $\bar{\beta}\approx 0.215$ to fit the SJM planar surface energy of Al, but this value of $\bar{\beta}$ results in an even larger curvature energy than that in Table I. In order to fit the EGM model to specific metals, the potential-well radius could be thus assumed to be a modified form, e.g., like $r=R+b+c/R$, where c is a specimen-dependent parameter. However, this could not be critical when one analyzes the shell structure and phase relations in electronic properties for a metal nanowire.

B. Shell structure

Now consider the oscillation features and phase relations in the electronic shell structure of a metal nanowire as well as the dynamic properties. The Fermi energy level ε_f versus R from Eq. (7) is plotted as the red solid curve in Fig. 3(a). The curve exhibits oscillatory damping around the bulk Fermi Energy E_F and the asymptotic behavior toward large radii is described well by Eq. (17), as indicated by the black solid curve in the inset of Fig. 3(a). At the subband (i.e., eigenenergy $\varepsilon_{n,|l|}$ crossing positions $\Xi_{I=1,2,\ldots}$, the curve is C^0 continuous (i.e., the curve is continuous but the corresponding first derivative discontinuous), and cusps appear as a series of local maxima. In contrast to metal nanofilms[8,10] for which the distance λ between any two neighboring cusps, i.e., the oscillation period, is approximately a constant value $\sim\lambda_F/2$, the oscillation "period" λ for metal nanowires is radius dependent, as shown in Fig. 3(a).

The surface free energy $\gamma=E-N\sigma_{\text{bulk}}$ calculated from Eq. (11) with Eqs. (6) and (9) is plotted in Fig. 3(b). As R increases, γ exhibits decaying oscillations. The asymptotic behavior toward large radii agrees well with the formula of Eq. (22), as indicated by the black solid curve in the inset of Fig. 3(b). While γ ultimately approaches the bulk film value γ_{bulk}, we can see significant deviation from the bulk value even as far as $R\sim 4\lambda_F$, suggesting importance of the curvature energy term. This result is in very good agreement with the calculations based on the SJM.[21] In addition, beats appear on the γ curve, which have been previously described as the superposition of a couple of dominant orbital frequencies from the Fourier analysis with a semiclassical model.[18,22]

An important difference between the curves of γ and ε_f versus R is that on the γ curve, the γ values at the positions $\Xi_{I=1,2,\ldots}$ correspond to a series of left inflexions of local maxima instead of the cusps on the ε_f curve. For nanofilms where the oscillation is approximately periodic, this gives rise to an offset by $\sim\lambda/4$ in the oscillation phases of γ and ε_f. This phase relation can also be confirmed from the synchronization between the curves of ε_f and γ' [the first derivative of γ with respect to Ξ, plotted in Fig. 3(c)] versus R. The γ curve at the subband crossings is C^1 continuous, i.e., γ' is continuous but the corresponding second derivative γ'' discontinuous, as shown in Figs. 3(c) and 3(d). The value of γ'' can reflect the thermodynamic stability of a nanowire. A generalized Nichols-Mullins model[38] for surface diffusion predicts that the stability coefficient is proportional to $S=\gamma''+\gamma'/R-\gamma/R^2\approx\gamma''$ for longitudinal perturbations. If $S>0$, the corresponding nanowire is stable, and if $S<0$, the nanowire is unstable. An expression equivalent to this criterion [cf. Eq. (7) in Ref. 29] is also obtained previously by Zhang *et al.* In terms of such criterion, from Fig. 3(d), the stable radii (in unit of λ_F) lie in the ranges (0.20, 0.36), (0.47, 0.59), (0.66, 0.68), (0.72, 0.80), (0.86, 0.92), (0.96, 1.01), (1.05, 1.14),…, and other radii are unstable. Generally, two ends of a metal nanowire fabricated in experiments[11,12,17–19] are in good electrical contact with two macroscopic metal electrodes, i.e., the nanowire can behave as an open system with exchange of electrons between the nanowire and the electrodes. For metal nanowires with good conductivity, Coulomb interactions lead to charge screening so that the local charge neutrality is a good approximation even for a relatively short nanowire,[39] and thus the nanowire can be approximately treated as a closed system. Charge fluctuations and screening effects are also investigated by Kassubek *et al.*,[40] who shows that for the nanowires with poor conductivity or large capacitance, charge screening can be weak, and then the effects of boundaries cannot be neglected. In the Au nanowire fabrication experiments of Kondo and Takayanagi[11] as well as Oshima *et al.*,[12] the observed stable radii (in unit of $\lambda_{F,\text{Au}}=0.52$ nm) are around the values of 0.38, 0.56, 0.85, 0.92, 0.99, 1.09, 1.15,… No stable nanowires are observed in some regions (i.e., the instability gaps), e.g., noticeably at the ranges (0.40, 0.50) and (0.58, 0.72). Note that the tiny stable range (0.66, 0.68) from Fig. 3(d) is not significant due to the corresponding small γ'' values. Thus, the thermodynamic stability from the model is in good agreement with that from the experiments. Since the stability pattern of a metal nanowire mainly originates from the oscillatory part in the surface energetics, the stable radii and instability gaps predicted from the above canonical-ensemble model is basically identical to the results obtained previously by Zhang *et al.* using the grand-canonical-ensemble model.[29–31] In their model, the effects of temperature and noncylindrical geometrical deformation of a metal nanowire are also included.

Next we describe the behavior of electron density. Figure 4(a) shows the three-dimensional (3D) plot of electron-density distribution $w(\rho)$ versus nanowire radius R from Eq. (10). For any nanowire with a fixed R, w oscillates as the function of ρ, exhibiting the Bardeen-Friedel oscillations,[41] which are induced by the metal-vacuum surface, while for any fixed position ρ, w oscillates as the function of R, exhibiting the QSE-induced oscillations. As two typical curves, the surface electron density $w(\rho=R)$ and the center electron density $w(\rho=0)$ versus R are plotted in Fig. 4(b). All of them have the cusps with the same positions as that of ε_f, as marked by the vertical green lines in Figs. 3 and 4(b). For $w(\rho=0)$, there is a remarkable oscillation feature that the

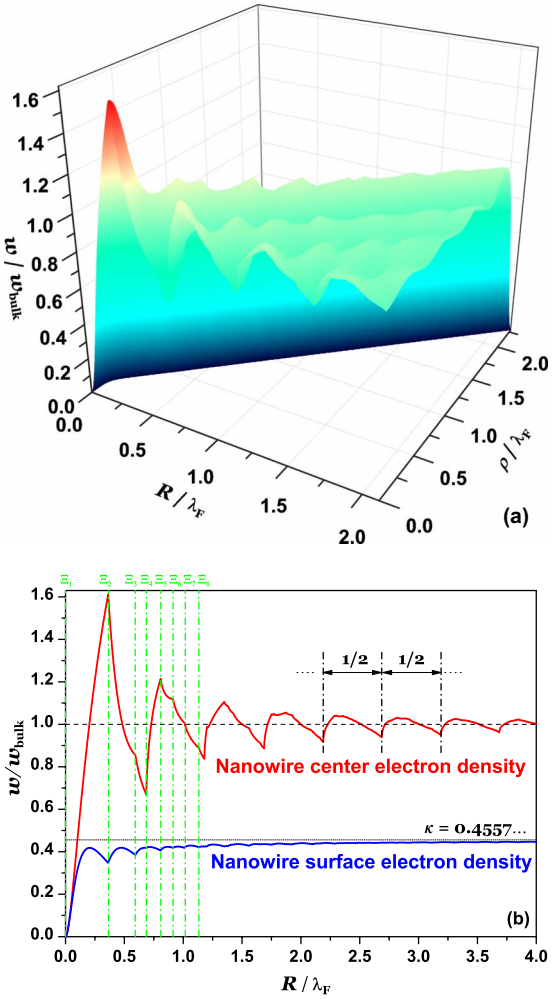

FIG. 4. (Color online) (a) The 3D plot of electron-density distribution $w(\rho)$ versus nanowire radius R from Eq. (10). (b) Electron densities w at the center and the geometric surface of nanowires versus R. Subband crossings are marked by green vertical dashed-dotted lines. Constant κ is the electron density at the geometric surface for a bulk film (Ref. 10).

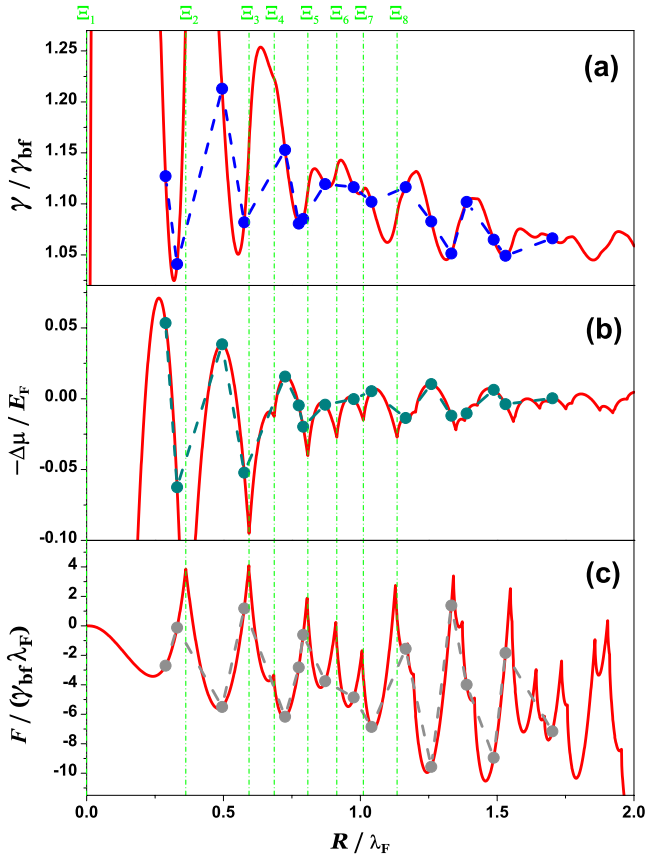

FIG. 5. (Color online) (a) Surface free energy γ, (b) $-\Delta\mu$ (negative increment of chemical potential relative to the bulk limit), and (c) elongation force F versus nanowire radius R. Subband crossings are marked by green vertical dashed-dotted lines. Dots on the curves correspond to the R values available according to Jia *et al.*'s DFT optimization calculations for Na helical nanowires (Ref. 15).

"global" oscillation period is equal to $\sim\lambda_F/2$, as shown in Fig. 4. The global minima on the red curve in Fig. 4(b) correspond to the quantum numbers $(l=0,n)$, $n=1,2,3,\ldots$ from small to big. Note that in term of the diameter, the period is $\sim\lambda_F$, being consistent with results for metal nanofilms.[10] For $w(\rho=R)$, the oscillatory curve [the blue curve in Fig. 4(b)] gradually approaches to the constant $\kappa=0.4557\ldots$, the electron density at the geometric surface for a bulk film [cf. Fig. (a) in Ref. 10].

The Fermi energy level ε_f is thermodynamically equivalent to the chemical potential μ. Because of the infinite potential-well barrier used in this model, we cannot calculate directly the work function W of a metal nanowire. Instead, we calculate the negative increment of chemical potential relative to the bulk limit: $-\Delta\mu=-(\mu-\mu_\infty)=E_F-\varepsilon_f$, which can be viewed as the "work function relative to the bulk limit."[9] In order to visualize the phase relations, we plot the curves (red solid) of γ and $-\Delta\mu$ versus R in Fig. 5(a) [the same as Fig. 3(b)] and Fig. 5(b), respectively. There is again an offset by $\sim\lambda/4$ in the oscillation phases of γ and $-\Delta\mu$, as indicated by the green vertical dashed-dotted lines denoting the subband crossings. This is obvious because the phases of $-\Delta\mu$ and ε_f are opposite according to the definition of $-\Delta\mu$. It should be mentioned that for a (more "realistic") soft-wall effective potential $U_{\text{eff}}(\rho)$, the work function should be expressed as $W=\Delta U_{\text{eff}}-\varepsilon_f$, where $\Delta U_{\text{eff}}=U_{\text{eff}}(\rho=\infty)-U_{\text{eff}}(\rho=0)$, which is the effective potential difference between at infinity and at the nanowire center. In principle, the effective potential U_{eff} could be obtained by self-consistently calculating the electron density and therefore the electrostatic potential plus the exchange-correlation part.[8] Generally speaking, ΔU_{eff} could be also oscillatory as a function of the size of a nanostructure (e.g., nanofilm or nanowire). Therefore, in order to understand the phase relation between W and $-\Delta\mu$ as well as other electronic properties, the specific self-consistent calculations are desirable.

Let us also examine the elongation force of a metal nanowire. When a nanowire elongates, we assume that the "geometric" or "jellium-background" volume V is conserved. In terms of the surface free energy γ, the elongation force F is given as a function of the wire radius R as[21]

$$F = -\left.\frac{dE}{dL}\right|_V = -\left.\frac{d(2\pi RL\gamma)}{dL}\right|_V = -\pi R\gamma + \pi R^2\frac{d\gamma}{dR}, \tag{24}$$

which is shown in Fig. 5(c). The fluctuation of the elongation force F can be calculated as

$$\delta F = F - \left[-\frac{d(2\pi RL\gamma_{\rm bf})}{dL}\right] = F + \pi R\gamma_{\rm bf}, \tag{25}$$

in which the second term is due to the increase in the surface area when the nanowire elongates and is considered as a bulk wire. The curve (red solid) of F versus R in Fig. 5(c) is in good agreement with the results from Zabala *et al.*'s SJM calculations for Al, Na, and Cs nanowires (see Fig. 5 in Ref. 21). Again, the agreement for Na and Cs is remarkable, indicating that for low electron densities, the noninteracting electron-gas model is an excellent approximation to the interacting jellium model. From Fig. 5, the phases of F and $-\Delta\mu$ are opposite, and thus there is also an offset by $\sim\lambda/4$ in the oscillation phases of γ and F. Here we also note that the elongation force and its fluctuation from Eqs. (24) and (25) are very similar to results obtained previously in the grand-canonical ensemble.[24,25,27]

It is possible to verify the above-predicted phase relations by either measuring experimentally or calculating from DFT the elongation force F, the work function W, and the thermodynamic stability. The latter is characterized by surface free energy γ, string tension f, or per electron energy σ, and these three quantities can be shown to possess the same phase, while ε_f, $-\Delta\mu$, and F have the identical or opposite phase [cf. Figs. 3(a), 5(b), and 5(c)]. For a metal electron-gas nanowire, the radius R is allowed to be continuous, as discussed above. For a real metal nanowire, the radius R is discrete, and these allowable values of R depend on the type of metal. For example, according to Jia *et al.*'s first-principles DFT optimization calculations for Na helical nanowires,[15] the relatively favorable configurations can be determined, and the corresponding discrete radii are marked in Fig. 5 (as well as Fig. 7 below) by the dots on the curves. Thus, from our present electron-gas model, γ, $-\Delta\mu$, and F of these Na helical nanowires will follow the dotted values connected with blue, green, and gray dashed curves, as shown in Figs. 5(a)–5(c), respectively.

The above analysis focuses on a closed system. The metal nanowires were also studied as an open system by using the free-electron model.[24–29] Although the overall shell structures from the closed and open systems are similar, we note that in calculations of thermodynamic properties, various assumptions about the compressibility of electron gas during its deformation can lead to significant difference in macroscopic properties. Besides the curvature energy discussed in Sec. III A, we find that for incompressible electron gas, the subband crossings always correspond to the inflection points on the surface-free-energy curve versus radius; for completely compressible electron gas in an open system, the subband crossings correspond to the cusp positions on the surface-free-energy curve versus radius (curves not shown here).

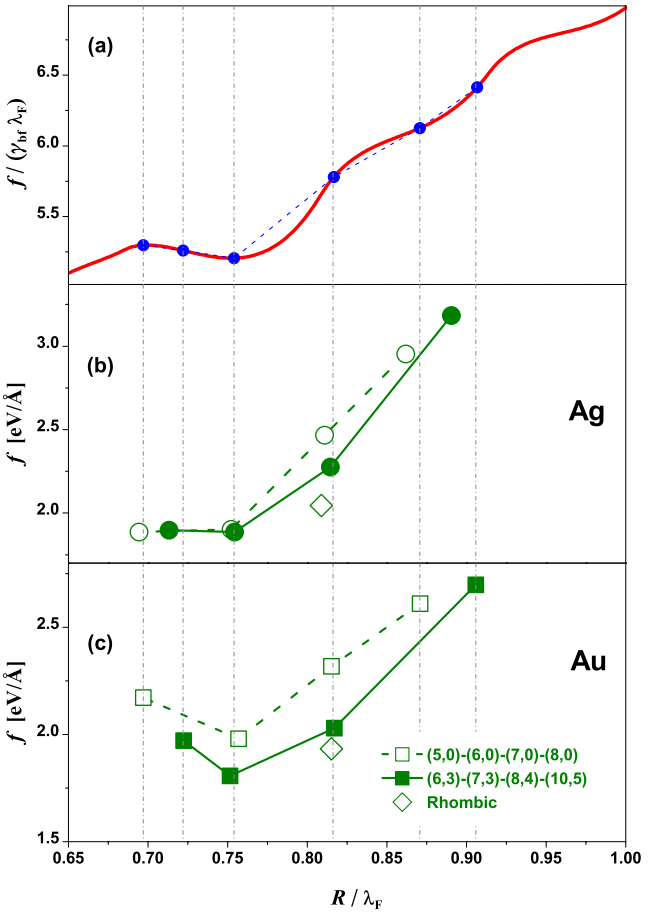

FIG. 6. (Color online) String tensions versus nanowire radius R. Red solid curve in (a) is obtained from $f=2\pi R\gamma$, where γ has been already plotted in Fig. 3(b). Data points in (b) and (c) are from DFT calculations in Ref. 14 for Ag and Au nanowires with different radii and configurations, respectively. Except the red solid curve in (a), all other lines are to guide the reader's eyes. Blue dots on the red solid curve correspond to the R values available in above DFT calculations, as marked by gray vertical lines. For all nanowire configuration details, see Ref. 14.

C. Comparison of results from EGM and DFT

To demonstrate the usefulness of the EGM for ultrathin nanowires, let us also compare the results of the EGM with first-principles DFT calculations existing in literature. Since DFT calculations are performed for closed systems, we therefore use the constant-b model here. The string tension $f=2\pi R\gamma$ is shown as the red solid curve in Fig. 6(a). The string tensions from empirical-potential plus DFT optimization calculations by Tosatti *et al.*[14] for Ag and Au nanowires with different radii and configurations are shown in Figs. 6(b) and 6(c), respectively. The agreement between the red solid curves and the available DFT data points is striking. Especially, the helical configuration (7,3) for Ag or Au nanowire corresponds to a local minimum of the red curve, indicating its magic stability.

The per electron energy σ versus nanowire R is plotted as the red solid curve in Fig. 7(a), which is compared with the average binding energy per atom from empirical-potential plus first-principles DFT optimizations by Jia *et al.*[15] for Na

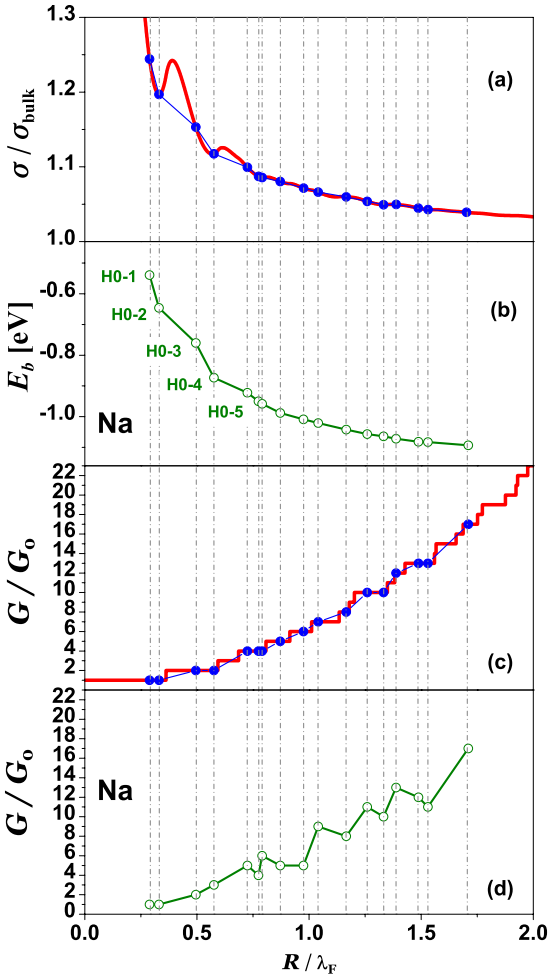

FIG. 7. (Color online) (a) Per electron energy versus R from $\sigma=E/N$ with N and E expressed in Eqs. (6) and (9), respectively. (b) Average (per atom) binding energy E_b versus R from first-principles DFT calculations in Ref. 15 for Na nanowires with different radii and configurations. (c) Conductance G versus R from Eq. (26). (d) Conductance G versus R from the same DFT calculations as in (b). Except the red solid curves, all other lines are to guide the reader's eyes. Blue dots on the red solid curves correspond to the R values available in above DFT calculations, as marked by gray vertical lines. For all nanowire configuration details, see Ref. 15.

helical nanowires (more favorable than other configurations) with different radii. The agreement between the red solid curve and these DFT data points is also striking. According to Jia *et al.*'s DFT optimization calculations,[15] no stable configurations can be found between two radii of H0-2 and H0-3 as well as of H0-4 and H0-5. This is consistent with the red solid curve in Fig. 7(b), where the parts of the curve corresponding to these radius regions are around the maxima of the curve.

Here we also mention that if the charge-neutrality requirement is ignored, i.e., b is simply set to be zero, the significant deviations from the curves of various physical properties versus radius will appear. For example, as discussed in Sec. III A, the surface free energy γ is very sensitive to the choice of b. From Eqs. (20) and (21), the asymptotic curve toward large radii for $b=0$ becomes $\gamma=\gamma_{bulk}(5+0.7997/\Xi)$ [cf. Eq. (22)]; also, when $b=0$, the curve of σ versus R (not shown) *does not exhibit any oscillations* [cf. Fig. 7(a) for $b=3\lambda_F/16$] so that there are no minima or maxima on the curve. Therefore, an appropriate choice of b satisfying the charge-neutrality requirement is important, as discussed in Sec. II.

Finally, we briefly explore a transport property. According to Landauer's multichannel formula,[42] the conductance G can be roughly estimated by

$$G/G_0 \approx \sum_{j=1}^{I} j = \frac{I(I+1)}{2}, \tag{26}$$

where $G_0 \equiv 2e^2/h$ is the quantum of conductance. Thus, the curve of G versus R is simply stepwise, as shown in Fig. 7(c). This is reasonably consistent with the results [Fig. 7(d)] from Jia *et al.*'s DFT calculations for Na nanowires.[15]

IV. CONCLUSION

In conclusion, an electron-gas model has been developed to investigate the oscillation behavior of various physical properties for a metal nanowire. Analysis of the model reveals that the electronic shell structure induces oscillations in various electronic properties with different phases. The basic behavior exhibited by our electron-gas model can be understood in terms of a correspondence between the local maxima (cusps) in the Fermi energy (which is related to the chemical potential or work function) and the inflection points located at the left of the local maxima of the surface free energy, as shown in Fig. 3. The model also predicts an oscillatory feature of electron density versus radius at the nanowire center with a global oscillation period which approximately equals half Fermi wavelength. By comparing with the previous free-electron models with constant chemical potential, we find that the main difference in our variable chemical-potential model is in the asymptotic behavior of surface energetics rather than the oscillatory features. In addition, the choice of potential-well boundary in the canonical ensemble or of constraints during deformation in the grand-canonical ensemble can also sensitively affect the asymptotic behavior, as noted previously by Urban *et al.*[31] within a grand-canonical-ensemble free-electron model.

ACKNOWLEDGMENTS

Y.H. was supported for this work by NSF under Grant No. CHE-0809472. D.J.L. was supported by the Division of Chemical Sciences of the U.S. DOE-BES. Computational supports at NERSC and TeraGrid were provided by U.S. DOE and NSF, respectively. We thank James W. Evans for a critical reading of the manuscript. We are also grateful to C. A. Stafford, Frank Kassubek, and Jérôme Bürki, as well as Daning Shi, for sharing their data. The work was performed at Ames Laboratory which is operated for the U.S. DOE by Iowa State University under Contract No. DE-AC02-07CH11358.

*octavian2009@gmail.com

[1] W. D. Knight, K. Clemenger, W. A. de Heer, W. A. Saunders, M. Y. Chou, and M. L. Cohen, Phys. Rev. Lett. **52**, 2141 (1984).
[2] K. Clemenger, Phys. Rev. B **32**, 1359 (1985).
[3] M. L. Cohen and W. D. Knight, Phys. Today **43**(12), 42 (1990).
[4] W. A. de Heer, Rev. Mod. Phys. **65**, 611 (1993).
[5] M. Brack, Rev. Mod. Phys. **65**, 677 (1993).
[6] T. P. Martin, Phys. Rep. **273**, 199 (1996).
[7] V. Lindberg and B. Hellsing, J. Phys.: Condens. Matter **17**, S1075 (2005).
[8] F. K. Schulte, Surf. Sci. **55**, 427 (1976).
[9] T. Miller, M. Y. Chou, and T.-C. Chiang, Phys. Rev. Lett. **102**, 236803 (2009).
[10] Y. Han and D.-J. Liu, Phys. Rev. B **80**, 155404 (2009).
[11] Y. Kondo and K. Takayanagi, Science **289**, 606 (2000).
[12] Y. Oshima, A. Onga, and K. Takayanagi, Phys. Rev. Lett. **91**, 205503 (2003).
[13] O. Gülseren, F. Ercolessi, and E. Tosatti, Phys. Rev. Lett. **80**, 3775 (1998).
[14] E. Tosatti, S. Prestipino, S. Kostlmeier, A. D. Corso, and F. D. D. Tolla, Science **291**, 288 (2001).
[15] J. Jia, D. Shi, B. Wang, and J. Zhao, Phys. Rev. B **74**, 205420 (2006).
[16] Y. Han, Fron. Phys. China **3**, 436 (2008).
[17] N. Agraït, G. Rubio, and S. Vieira, Phys. Rev. Lett. **74**, 3995 (1995).
[18] A. I. Yanson, I. K. Yanson, and J. M. van Ruitenbeek, Phys. Rev. Lett. **84**, 5832 (2000).
[19] A. I. Mares and J. M. van Ruitenbeek, Phys. Rev. B **72**, 205402 (2005).
[20] C. Yannouleas, E. N. Bogachek, and U. Landman, Phys. Rev. B **57**, 4872 (1998).
[21] N. Zabala, M. J. Puska, and R. M. Nieminen, Phys. Rev. B **59**, 12652 (1999).
[22] M. J. Puska, E. Ogando, and N. Zabala, Phys. Rev. B **64**, 033401 (2001).
[23] E. Ogando, N. Zabala, and M. J. Puska, Nanotechnology **13**, 363 (2002).
[24] C. A. Stafford, D. Baeriswyl, and J. Bürki, Phys. Rev. Lett. **79**, 2863 (1997).
[25] S. Blom, H. Olin, J. L. Costa-Krämer, N. García, M. Jonson, P. A. Serena, and R. I. Shekhter, Phys. Rev. B **57**, 8830 (1998).
[26] A. M. Zagoskin, Phys. Rev. B **58**, 15827 (1998).
[27] C. A. Stafford, F. Kassubek, J. Bürki, and H. Grabert, Phys. Rev. Lett. **83**, 4836 (1999).
[28] E. N. Bogachek, A. G. Scherbakov, and U. Landman, Phys. Rev. B **62**, 10467 (2000).
[29] C.-H. Zhang, F. Kassubek, and C. A. Stafford, Phys. Rev. B **68**, 165414 (2003).
[30] D. F. Urban, J. Bürki, C.-H. Zhang, C. A. Stafford, and H. Grabert, Phys. Rev. Lett. **93**, 186403 (2004).
[31] D. F. Urban, J. Bürki, C. A. Stafford, and H. Grabert, Phys. Rev. B **74**, 245414 (2006).
[32] J. Bardeen, Phys. Rev. **49**, 653 (1936).
[33] M. Brack and R. K. Bhaduri, *Semiclassical Physics*, Frontiers in Physics Vol. 96 (Addison-Wesley, Reading, MA, 1997).
[34] J. P. Perdew, Y. Wang, and E. Engel, Phys. Rev. Lett. **66**, 508 (1991).
[35] J. P. Perdew, P. Ziesche, and C. Fiolhais, Phys. Rev. B **47**, 16460 (1993).
[36] P. Ziesche, M. J. Puska, T. Korhonen, and R. M. Nieminen, J. Phys.: Condens. Matter **5**, 9049 (1993).
[37] N. D. Lang and W. Kohn, Phys. Rev. B **1**, 4555 (1970).
[38] F. A. Nichols and W. W. Mullins, Trans. Metall. Soc. AIME **233**, 1840 (1965).
[39] J. M. van Ruitenbeek, M. H. Devoret, D. Esteve, and C. Urbina, Phys. Rev. B **56**, 12566 (1997).
[40] F. Kassubek, C. A. Stafford, and H. Grabert, Phys. Rev. B **59**, 7560 (1999).
[41] V. Sahni (private communication); also see Ref. 10, and *Quantal Density Functional Theory II: Approximation Methods and Applications* (Springer-Verlag, Berlin, 2010).
[42] R. Landauer, IBM J. Res. Dev. **1**, 223 (1957).